Cleaner Waste Systems 4 (2023) 100081

Contents lists available at ScienceDirect

Cleaner Waste Systems

journal homepage: www.journals.elsevier.com/cleaner-waste-systems

# Phosphorous removal from human urine using lateritic soil

Austine O. Otieno[a,b,*], Patrick G. Home[a], James M. Raude[a], Sylvia I. Murunga[c], Gerryshom Munala[d], Dickson O. Ojwang[e], Tuula Tuhkanen[f]

[a] Soil, Water and Environmental Engineering Department (SWEED), Jomo Kenyatta University of Agriculture and Technology, P.O. Box 62000-00200, Nairobi, Kenya
[b] Department of Geoscience and the Environment (DGSE), Technical University of Kenya, P.O. Box 52428-00200, Nairobi, Kenya
[c] Agricultural and Biosystems Engineering Department (ABED), Jomo Kenyatta University of Agriculture and Technology, P.O. Box 62000-00200, Nairobi, Kenya
[d] Centre for Urban Studies, Jomo Kenyatta University of Agriculture and Technology, P.O. Box 62000-00200, Nairobi, Kenya
[e] Department of Chemistry – Ångström Laboratory, Uppsala University, Box 538, SE-751 21 Uppsala, Sweden
[f] Department of Biological and Environmental Science, University of Jyvaskyla, P.O. Box 35, FI-40014, Finland

ARTICLE INFO

*Keywords:*
Human urine
Phosphorous adsorption
Adsorption isotherms
Response surface optimisation

ABSTRACT

Phosphorous (P) in human urine is among the macronutrients in municipal wastewater that has exacerbated eutrophication of water bodies. Adsorption of P from wastewater using cost effective, environmentally friendly, and efficient adsorbents is considered as an attractive method that can both mitigate the eutrophication problem and augment the already strained P reserves. In the present study the adsorption capacity and structural properties of lateritic soil (LS), the adsorbent for removal of P from human urine, was investigated using XRF, SEM, TGA and FTIR techniques. Batch adsorption experiments were conducted to determine various adsorption parameters such as the sorption rates, the concentration, and the amount of adsorbed P at equilibrium. The experimental equilibrium data were fitted to the Langmuir, Freundlich and Dubinin-Radushkevich (D-R) adsorption isotherms. Also, factors influencing adsorption such as the contact time, agitation speed, and adsorbent loading were optimized using response surface methodology (RSM). Based on the D-R model, mean surface adsorption energy of $1.313 \times 10^{-2}$ kJ/mol was obtained suggesting that the adsorption occurred through weak forces of interaction. The amount of adsorbed P on LS at equilibrium ($q_e$) and pH = 7.5 increased with the initial concentration of P in urine as well as with the contact time. The Langmuir maximum adsorption of P on LS was found to be 15.5 mg/g. The RSM demonstrated that contact time 60 min, agitation speed 80 rpm, and adsorbent loading 0.1 g in 25 mL of urine were optimum for the highest adsorption of P, and a desirability of 0.919. The results presented here show that LS is a promising inexpensive adsorbent for effective removal of P from human urine.

## 1. Introduction

Phosphorous (P) is one of the most important macronutrient elements for the growth of terrestrial and aquatic plants and microorganisms. However, discharge of elevated concentrations of P from agricultural and domestic sources into aquatic environments has accelerated eutrophication, which has not only become a threat to the life of the aquatic creatures but also causes growing environmental concerns worldwide (Preisner et al., 2021). Discharge of wastewater from agro-industrial and municipal treatment plants to water bodies has led to increased loadings of phosphorous (Beusen et al., 2016). While high concentrations of P are harmful to the environment, it is widely used in fertilizer production, detergent manufacturing, and mineral processing. The typical raw domestic wastewater conveyed to centralized wastewater treatment plants contains human urine, which constitutes only ~ 1 % of the total volume. Despite urine taking only a small percentage of the domestic water, it has approximately 50–80 % phosphorous (Larsen and Gujer, 1996), which mainly exists in dissolved form as phosphates ($H_2PO_4^-$ or $HPO_4^{2-}$) (Udert et al., 2006). Although the conventional centralized wastewater treatment systems target to eliminate or minimize phosphates and other macronutrients, the high infrastructural cost, and large freshwater required for conveying the human excreta to treatment plants may inhibit their effective adoption in low income, and water scarce countries. Further, effluents from treatment plants in developing countries have high nutrient loads as a result of overloaded capacities due to rising urbanisation, design

* Corresponding author at: Soil, Water and Environmental Engineering Department (SWEED), Jomo Kenyatta University of Agriculture and Technology, P.O. Box 62000-00200, Nairobi, Kenya.
*E-mail address:* austine.otieno@tukenya.ac.ke (A.O. Otieno).

https://doi.org/10.1016/j.clwas.2023.100081
Received 1 August 2022; Received in revised form 18 January 2023; Accepted 2 February 2023

weaknesses, poor maintenance, and inefficient monitoring for compliance (Edokpayi et al., 2017). Thus, the concept of separation of human excreta at the source and treating them to recover valuable nutrients for crop production may provide the double benefit of recycling the non-renewable phosphorus resources from human urine, while also protecting aquatic ecosystems from eutrophication (Karak and Bhattacharyya, 2011; Wilsenach et al., 2007). Also, it is acknowledged that the need for removal and recovery of P from human urine is necessary given that non-renewable P resources such as phosphate rock reserves are gradually diminishing and will eventually be depleted (Van Vuuren et al., 2010).

During the past decades, methods such as chemical precipitation, biological treatment, ion-exchange, reverse osmosis, electrodialysis, and adsorption have all been explored towards the removal of P from water and wastewaters (Biswas et al., 2008; Boujelben et al., 2008; Jeppesen et al., 2009; Mohamed, 2002; Xu et al., 2011). The latter method can both remove and recover P, and it is the most economical, more efficient, and relatively simple to operate (Martin et al., 2020). Several adsorbents including, slag (Yamada et al., 1986), red mud (López et al., 1998), aluminium oxide (Tanada et al., 2003), fly ash (Oguz, 2005), crab shells (Jeon and Yeom, 2009), and zeolite (Wu et al., 2006) have been investigated for the removal of P from wastewater. In particular, the presence of aluminium (Al) and iron (Fe) cations in adsorbents is known to enhance their adsorption and chemical precipitation of P in wastewater (Bhattacharjee et al., 2021; Fulazzaky et al., 2014). For instance, the use of Al based drinking water treatment sludge for removing different phosphate species from wastewater has been reported to be effective (Chittoo and Sutherland, 2014; Razali et al., 2007; Yang et al., 2006). Acid mine drainage sludge has also been demonstrated to be efficient in the removal of P from municipal wastewater treatment plant effluent due to the attraction of phosphates by the Al and Fe cations (Wei et al., 2008).

However, besides elemental composition, optimal adsorption of targeted nutrients from a solution is greatly affected by other adsorbent properties such as surface area, ion-exchange capacities, and porosity (Yadav et al., 2017). These properties vary among materials depending on their morphology, functional groups, inherent composition, and the synthesis conditions.

Lateritic soil (LS), represented in Fig. 1, is a low-cost naturally available clay commonly found in humid regions, and is highly rich in metal oxides of Fe and Al (Stoops and Marcelino, 2018) which play a fundamental role in the removal of P from aqueous phases.

**Fig. 1.** Pictorial representation of lateritic soil with characteristic reddish-brown color. Inset is an example of how the soil sample used in this study was stored in an airtight vial for characterization.

Most of the studies on the use of LS for adsorption have mainly focused on the removal of fluorides (Osei et al., 2016; Sarkar et al., 2006), and heavy metals (Glocheux et al., 2013; Mitra et al., 2016) from water or wastewaters. An investigation on its application for the removal of $PO_4^{3-}$ from wastewater is very recent (Bhattacharjee et al., 2021). The concentrations of $PO_4^{3-}$ in human urine are orders of magnitude greater than in the domestic wastewater (Maurer et al., 2006), and so determining the LS adsorption capacity in natural human urine would be important to optimize its use for the removal of phosphorous. Also, determining the mechanism of sorption of P on LS will provide an insight on the surface properties of LS.

To date, adsorption isotherm models have been widely used in investigating the sorption properties of adsorbents in aqueous solutions in order to determine the capacity of a particular adsorbent for removal of the intended ions or molecules in solutions (Ayawei et al., 2017). Both linear and nonlinear regression methods have been very often used in fitting the equilibrium adsorption data to the known adsorption isotherm models (Yaneva et al., 2013). However, growing discrepancy have been observed between the predictions and experimental data when linear regression methods are used in fitting the equilibrium adsorption data to the isotherm models leading to unreliable estimates of the model parameters (Foo and Hameed, 2010). Thus, researchers (Abdullah et al., 2009; Yaneva et al., 2013) have reported that expanding the nonlinear isotherms represents a potentially viable and powerful tool, which could lead to an improvement in the area of adsorption science.

In this work we have made an effort to understand the sorption properties of a low-cost and abundantly available LS during the removal of P from human urine. To our knowledge the phosphorous sorption properties of LS in human urine have not been reported before. The elemental composition, surface morphology, functional groups, and thermal stability of the material have been investigated to assess its potential for the adsorption of P. Batch adsorption experiments and equilibrium isotherm modeling based on the nonlinear Langmuir, Freundlich, and Dubinin-Radushkevich (D-R) equations have been performed to examine the adsorption capacity, and the adsorption mechanism of P on LS. In addition, the effect of contact time and the initial concentration of P adsorption process have been explored. Finally, response surface methodology (RSM) has been used to obtain the optimal conditions of contact time, agitation speed, and adsorbent loadings for enhancing the adsorption of P on LS.

## 2. Materials and methods

### 2.1. Materials

Human urine was collected from volunteers and used directly without further purification. Lateritic soil was excavated 20 cm from the ground surface, and impurities such as leaves and roots removed. The soil was then dried in an oven at 104 ± 1 °C for 24 h under vacuum. The dried soil was then crushed, sieved to ≤ 300 μm and kept in an airtight vial for further studies.

### 2.2. Materials characterization

Human urine was characterized for pH and temperature using a Mettler Toledo SevenEasy S20 pH meter. Procedure used in determination of concentration of P in the urine is detailed in Section 2.3. The elemental composition of lateritic soil was determined using a Bruker S1 Titan 500 X-ray fluorescence (XRF) spectrometer. The thermal stability, and dehydration temperature were determined using a TGA-Q500 thermogravimetric analyzer (TA Instruments). Approximately 5 mg of the soil sample powder was heated from 30 to 800 °C at a rate of 5 °C/min under flowing $N_2$ gas. To determine the main functional

groups an attenuated total reflectance Fourier transform–infrared (ATR-FTIR) spectroscopic technique was performed using a Spectrum One spectrometer. The spectrum was obtained in the range of 4000–650 $cm^{-1}$ by averaging 40 scans at a spectral resolution of 4 $cm^{-1}$. A LEO 1550 scanning electron microscope (SEM) was used to study the sample morphology. SEM images were recorded at an acceleration voltage of 1 kV, and a working distance of ~ 4.5 mm. Sample powders were dispersed on a double-sided carbon tape and mounted on an aluminium stub prior to the analysis. A more extensive report on the preparation and structural determination of the compounds has been published by Otieno et al. (2021).

### 2.3. Analytical methods

Phosphorous (P) in the human urine samples was determined according to Finnish standard Finnish standard (SFS, 3026) for determination of total phosphorous in water (Finnish Standards SFS 3026, 1986).

#### 2.3.1. Preparation of phosphorous stock solution and working standards

Phosphorous stock solution (50 mg/L P) was prepared by dissolving 0.2197 g of dry potassium di-hydrogen phosphate ($KH_2PO_4$) in deionized (DI) water. 10 mL of 4 M $H_2SO_4$ was then added, and the solution diluted to a total volume of 1000 mL. Phosphorous working solution (1/50 dilution of the stock solution) was prepared by diluting 10 mL of the stock solution with DI water to a total volume of 500 mL.

#### 2.3.2. Procedure for obtaining calibration curve of phosphate and calculating concentrations of phosphate in human urine

The first step in the SFS 3026 method for determining concentrations of phosphate was to develop the standard calibration curve using five working standards. In this method, calibration standards are prepared by pipetting different amounts (1, 2, 10, 25 and 75 mL) of phosphate working solution into 100 mL volumetric flasks. They are then acidified with 1 mL of 4 M $H_2SO_4$ and diluted with DI water to the 100 mL mark. The calibration solutions therefore contained 10, 20, 100, 250 and 750 μg/L of P. Blank or zero samples were also prepared by pipetting 10 mL of 4 M $H_2SO_4$ in 1000 mL volumetric flask and then adding DI water to the 1000 mL mark. Each sample investigated was prepared in three replicates. 5 mL of potassium persulfate (5 g $K_2S_2O_8$ per 100 mL DI water) solution was added into each bottle to transform phosphorous into phosphates. The bottles were autoclaved at 120 °C for 40 min to expedite the transformation process and then cooled to room temperature, 21 ± 1 °C. 1 mL of each ascorbic acid ($C_6H_8O_6$) and ammonium molybdate ($(NH_4)_6Mo_7O_{24}$) reagents were then added for color development. UV-Spectrophotometer (880 nm wavelength) was used to obtain the total P readings. The absorbance and concentration values of blank (zero) samples were read first followed by absorbance of the standards whose concentration had been predetermined in the experiment. The plot of absorbance against concentration of the blanks and the standards gave a calibration curve from which the concentration of P in the samples of unknown concentration was calculated based on the absorbance readings obtained by the spectrophotometer.

For the human urine whose concentrations of P were unknown, 0.5 mL of urine samples from the original urine samples (control) and the adsorption experiment (filtrate) were pipetted into 500 mL volumetric flasks, acidified with 5 mL of 4 M $H_2SO_4$ then topped with DI water to the 500 mL mark. 25 mL of each of the prepared samples were transferred into clean autoclave bottles. Subsequent procedures already described earlier in this section (addition of persulfate, autoclaving, color development) were then followed, and the absorbance reading obtained from the spectrophotometer used to calculate the concentration of the urine samples from the calibration curves.

### 2.4. Batch adsorption studies

Six different concentrations of P 164.12, 283.55, 309.82, 439.95, 555.04, and 680.21 mg/L at 21 °C, and pH = ~ 7.50 ± 0.30, were obtained by diluting the original urine sample with DI water. 25 mL of urine was placed in each 250 mL conical flask and dosed with 0.2 g of lateritic soil adsorbent. The samples were agitated continuously at 100 rpm for 30, 60, 90, and 120 min, respectively, with a laboratory shaker (Heidolph unimax orbital shaker 2010, Germany). The experiments were conducted in three replicates for each contact time and initial concentration. The adsorbent was separated from the urine solution through filtration using Whatman filter paper no. 42. The amount of adsorbed P was calculated using Eq. (1)

$$q_t = \frac{(C_o - C_t)V}{W} \quad (1)$$

where, $C_o$ and $C_t$ (mg $L^{-1}$) are the concentrations of P in the urine at the initial time, and at a certain time $t$, respectively, $V$ (mL) is the volume of urine, $W$ (g) is the mass of adsorbent and $q_t$ (mg/g) is the amount of adsorbed P per unit mass (g) of the adsorbent.

### 2.5. Adsorption isotherms

The analysis of the adsorption data is important to develop equations which accurately represents the results and that could be used for design purposes. This is commonly done by fitting the adsorption data to adsorption isotherms. Three equilibrium isotherms, the Langmuir, Freundlich, and Dubinin-Radushkevich (D-R) models were fitted in order to investigate the adsorption behavior of P on the lateritic soil.

#### 2.5.1. Langmuir model

This model assumes that adsorption occurs in monolayer on active sites with same adsorption energies (Ayawei et al., 2017). Its nonlinear form (Foo and Hameed, 2010) is given as in Eq. (2)

$$q_e = \frac{q_m K_L C_e}{1 + K_L C_e} \quad (2)$$

where, $q_e$ (mg/g) is the amount of adsorbed P at equilibrium, $C_e$ (mg/L) is the equilibrium concentration of P, $q_m$ (mg/g) is the saturated monolayer adsorption capacity, $K_L$ (L/mg) represents the binding energy between the adsorbate and the adsorbent. The plot of experimental and model $q_e$ against $C_e$ gives a nonlinear plot.

The Langmuir model constant ($K_L$), can further be used to compute the dimensionless separation factor ($R_L$) according to Eq. (3)

$$R_L = \frac{1}{1 + K_L C_o} \quad (3)$$

where, $C_o$ (mg/L) is the initial concentration of P in the solution, $K_L$ (L/mg) is the Langmuir constant, $R_L$ is a dimensionless separation factor. If $R_L$ is in the range between 0 and 1, then the adsorption process is considered favorable (Hameed and El-Khaiary, 2008).

#### 2.5.2. Freundlich model

This model is based on the assumption that adsorption occurs in multilayer on heterogeneous adsorption sites (Ayawei et al., 2017). Its nonlinear form (Foo and Hameed, 2010) is expressed as in Eq. (4)

$$q_e = K_f C_e^{1/n} \quad (4)$$

where, $q_e$ (mg/g) is the amount of adsorbed P at equilibrium, $C_e$ (mg/L) is the equilibrium concentration of P, $K_f$ and $1/n$ are constants incorporating the factors affecting the adsorption capacity and adsorption intensity, respectively. The plot of experimental and model $q_e$ against $C_e$ gives a nonlinear plot.

*2.5.3. Dubinin-Radushkevich (D-R) model*

The D-R model is often employed to determine whether an adsorption process is chemical or physical based on the mean surface adsorption energy (Mahmoud, 2015). Its nonlinear form (Foo and Hameed, 2010) is expressed as in Eq. (5)

$$q_e = q_s \exp(-K_{DR}\varepsilon^2) \quad (5)$$

where, $q_e$ (mg/g) is the amount of adsorbed P at equilibrium, $qs$ (mg/g) is the theoretical isotherm saturation capacity, $-K_{DR}$ (mol$^2$/kJ$^2$), and ε are Dubinin-Radushkevich (D-R) model parameters. The constant ε is calculated according to Eq. (6)

$$\varepsilon = RT \ln(1 + 1/C_e) \quad (6)$$

where, $R$ is the universal gas constant (8.314 J/mol K), $T$ is the temperature (Kelvin), $C_e$ (mg/L) is the equilibrium concentration of P. The plot of experimental and model $q_e$ against $C_e$ gives a nonlinear plot.

The mean surface adsorption energy (E) (kJ/ mol) is calculated using Eq. (7) (Hu and Zhang, 2019)

$$E = \frac{1}{\sqrt{2K_{DR}}} \quad (7)$$

The adsorption process is considered physical if $E < 8$ kJ/mol, whereas chemisorption occurs if $E > 18$ kJ/mol (Mahmoud, 2015).

It is worth noting that, a trial-and-error nonlinear regression method, which is applicable to computer operation, were used to compare the best-fitting of the three isotherms using an optimization routine to maximize the coefficient of determination $R^2$, between the experimental, and isotherms data in the solver add-in with Microsoft Excel spreadsheet (Yuh-Shan, 2006). The coefficient of determination $R^2$ is defined as shown in Eq. (8).

$$R^2 = 1 - \frac{(\bar{q}_e - \bar{q}_m)^2}{\sum (q_e - q_m)^2} \quad (8)$$

where $q_e$ (mg/g) is the equilibrium capacity obtained from experiment, $q_m$ (mg/g) is the equilibrium capacity obtained from the isotherm model, $\bar{q}_e$, and $\bar{q}_m$ is the average of $q_e$, and $q_m$, respectively.

*2.6. Response surface methodology (RSM) experimental design and evaluation*

Response surface methodology (RSM) coupled with central composite circumscribed design (CCCD) as described by Myers et al. (2004), was employed to optimize the adsorption of P on lateritic soil and to investigate the interactive effects of contact time ($x_1$, min), agitation speed ($x_2$, rpm), and adsorbent loading ($x_3$, g) on the adsorption process of P. "Design-Expert® software, version 12, Stat-Ease, Inc., Minneapolis, MN, USA, www.statease.com" was used for designing and analyzing the experimental data. The coefficient of determination ($R^2$) was used to express the validity of the model, while adequacy or soundness of the model was evaluated by analysis of variance (ANOVA). For statistical calculations, the selected independent variables (contact time, agitation speed, and adsorbent loading) were coded as follows Eq. (9)

$$x_i = \frac{X_i - X_o}{\Delta X} \quad (9)$$

where, $x_i$ is the coded variable, $X_i$ is the un-coded value of the $i$th independent variable, $X_o$ is the value of $X_i$ at the center point of the investigation area, $\Delta X$ is the step change.

Each variable was studied at 5 levels coded as − 1.682, − 1, 0, 1, + 1.682, where (− 1) is low level, (+ 1) is high level, (0) is the center point, ± 1.682 are codes for points defined by the design expert software to be below and above the respectively designated low and high levels in each factor studied. The parameters and levels for the experimental design used in this study are presented in Table 1.

The RSM model correlates the dependent variables to the independent variables considered through a second-order polynomial response equation given as in Eq. (10)

$$Y = \beta_o + \beta_1 x_1 + \beta_2 x_2 + \beta_3 x_3 + \beta_{12} x_1 x_2 + \beta_{13} x_1 x_3 + \beta_{23} x_2 x_3 + \beta_{11} x_1^2 + \beta_{22} x_2^2 + \beta_{33} x_3^2 + \varepsilon \quad (10)$$

where, $Y$ is the predicted response (in this case the amount of adsorbed P), $\beta_o$ is the value of the fixed response at the center point of the design, $\beta_i (i = 1,2,3)$, $\beta_{ii} (ii = 11,22,33)$and $\beta_{ij} (ij = 12,13,23)$ are the linear, quadratic and interaction effect regression terms, respectively, and $\varepsilon$ is the random error.

The 3D response surfaces were then drawn to visualize the individual and the interactive effects of the independent variables on the adsorption of phosphorous, and results validated by conducting the experiment at the predicted optimal conditions. The 3D plots are provided in the Supplementary information. To perform numerical optimization for the adsorption of P on LS, the desirability function approach was followed. The desirability is a dimensionless entity that represents the closeness of a response to its ideal value and usually ranges from 0 to 1 with d = 0 being unacceptable, and d = 1 indicating that the model response is equal to that of the target value (Li et al., 2007; Myers et al. (2004)). In our study, the criteria setup for the RSM during the numerical optimization was to maximize the contact time, and minimize the agitation speed and adsorbent loading with the overall goal of maximizing the adsorbed P on LS.

## 3. Results and discussion

*3.1. Composition and structure of lateritic soil (LS)*

The main components of lateritic soil as revealed by XRF data are $SiO_2$ = 55.83 wt%, $Al_2O_3$ = 20.02 wt%, and $Fe_2O_3$ = 9.50 wt% (Table 2). These results relate well with previous studies (Kamtchueng et al., 2015; Ko, 2014). The mineral phases detected by the XRF analysis corroborates the XRD data obtained by Otieno et al. (2021) where iron oxide, silicon oxide, and aluminum silicates were found to be the dominant components of LS.

The low amount of soluble alkaline oxides (CaO, $K_2O$, and $P_2O_5$) suggest that the soil had undergone extensive leaching making it acidic, and infertile for crop production (Kisinyo et al., 2014). The thermal stability illustrated in the TG-DTG curves (Fig. 2a), reveal the release of weakly adsorbed water at $T < 100$ °C, followed by decomposition of hemicellulose between 220 °C and 315 °C, and cellulose between 315 °C and 420 °C, while the rapid mass loss between 420 and 650 °C is typical of dehydroxylation of kaolinite (Kakali et al., 2001; Rocha and Klinowski, 1990). The sample morphology is composed of aggregated nanoparticles with size distribution in the range ~ 10–100 nm (Fig. 2a insert).

The FTIR adsorption bands for surface water appear at frequency values of 3630 cm$^{-1}$, 3590 cm$^{-1}$, and 3550 cm$^{-1}$ (symmetrical and asymmetrical O–H stretching vibrations) (Lemougna et al., 2014) as shown in Fig. 2b. The band around 2000 cm$^{-1}$ is assigned to the presence of adsorbed carbonyl groups. The band around 1600 cm$^{-1}$ corresponds to interlayer water molecules (H–O–H bending modes) in the framework of the adsorbent (Lemougna et al., 2014). The bands in the region 1200–700 cm$^{-1}$ are associated with Si-O-Fe, Si-O, Al-OH, and Fe-OH stretching vibrations, also observed for kaolinite–hematite composite. (Kakali et al., 2001; Rocha and Klinowski, 1990). The elements Al and Fe have been widely reported to form complexes with phosphate molecules thereby removing P from aqueous phases (Chittoo and Sutherland, 2014; Razali et al., 2007; Yang et al., 2006).

*3.2. Adsorption isotherms*

To describe the adsorption behavior of P on LS and estimate the adsorption maxima, the experimental data of the adsorption isotherms were modeled using the nonlinear Langmuir, Freundlich, and Dubinin-

**Table 1**
Parameters and levels for the experimental design.

| Independent variable | Symbol | Code factor levels | | | | |
|---|---|---|---|---|---|---|
| | | -1.682 | -1 | 0 | 1 | 1.682 |
| Contact time (min) | $x_1$ | 20 | 30 | 45 | 60 | 70 |
| Agitation speed (rpm) | $x_2$ | 39 | 80 | 140 | 200 | 241 |
| Adsorbent loading (g) | $x_3$ | 0.03 | 0.1 | 0.2 | 0.3 | 0.37 |

Radushkevich (D-R) equations. The Langmuir adsorption model assumes a monolayer adsorption on homogenous surfaces, while the Freundlich model assumes a multilayer adsorption on heterogeneous surfaces. The D-R model on the other hand can be used to distinguish between physisorbed and chemisorbed ions based on the mean adsorption energies of the available adsorption sites. The graphical plots of the adsorption isotherms of the three models are presented in Fig. 3.

The coefficient of determination ($R^2$) for Langmuir, Freundlich, and D-R models were 0.999, 0.996, and 0.999, respectively implying that the parameters obtained from the model were reliable in estimating the P adsorption behavior of LS in human urine. Also, the calculated mean surface adsorption energy ($E = 1.313 \times 10^{-2}$ kJ/mol) from the D-R model presented in Table 3 shows that P was bound on the LS surface by weak electrostatic (Van der Waal) forces since the value was below 8 kJ/mol (Hu and Zhang, 2019). Other studies (Bhattacharjee et al., 2021; Fulazzaky et al., 2014) have also reported that Al and Fe cations in LS are responsible for the removal of P from an aqueous phase through electrostatic attraction to form complexes. Thus, sorption mechanism is controlled by the chemical properties of the soil.

The adsorption capacities of different adsorbents are highly dependent on the operating temperatures, material surface area, and initial solution concentrations (Zhang et al., 2011). As shown in Table 4, it is evident that LS used in this study can adsorb a maximum of 18.0 mg/g P from human urine, which is in the typical range for many adsorbents; 9.8 mg/g for bentonites, 4.3 mg/g for wood aspen fibres, 41.97 mg/g for calcined alunite, and 36 mg/g for Fe-Mn binary oxide among others. The significantly high value of 384.61 mg/g reported in a very recent study by Bhattacharjee et al. (2021) on the adsorption of P from sewage effluent is very surprising, however, these authors did not provide a satisfactory explanation for the high discrepancy.

### 3.3. Influence of contact time on the adsorption of P on LS

The effect of contact time on the adsorption of P on LS was studied by dosing 0.2 g of the adsorbent in 25 mL of urine and shaking at 100 rpm for 30, 60, 90, and 120 min, respectively, at 21 °C, and pH of ~ 7.50 ± 0.30. As can be seen in Fig. 4, the capability of LS to adsorb P from human urine was profoundly influenced by the contact duration as exhibited by all the urine solutions with different initial concentrations of P.

As illustrated in Fig. 4 it is evident that the adsorption of P on LS mainly occurred in three stages. The adsorption of P was rapid within the first 30 min of contact time. This is attributable to a large number of vacant adsorption sites available. What follows is a gradual decline in the sorption rate between 30 and 90 min, which could be due to the adsorption sites being gradually occupied as the adsorption process continued. In the final step, the adsorption of solutes tends towards constant values beyond 90 min, suggesting saturation of the available sorption sites. Ragheb (2013) observed a similar trend when slag and fly ash was used to remove phosphate from aqueous solution. According to the author a rapid uptake occurred in the first 30 min of contact period but the amount of the adsorbed phosphates beyond 60 min remained constant. The ionic gradient influences adsorption such that the high difference in phosphate concentration between the solution and the adsorbents at the onset of adsorption process resulted into a higher rate of diffusion of the solutes through the pores of the adsorbent to the

**Table 2**
Chemical composition of LS from XRF analysis (wt%).

| $SiO_2$ | $Al_2O_3$ | CaO | $Na_2O$ | $K_2O$ | $TiO_2$ | MnO | $Fe_2O_3$ | $P_2O_5$ | S |
|---|---|---|---|---|---|---|---|---|---|
| 55.83 | 20.02 | 1.01 | 1.00 | 1.80 | 1.20 | 0.14 | 9.50 | 0.79 | 0.18 |

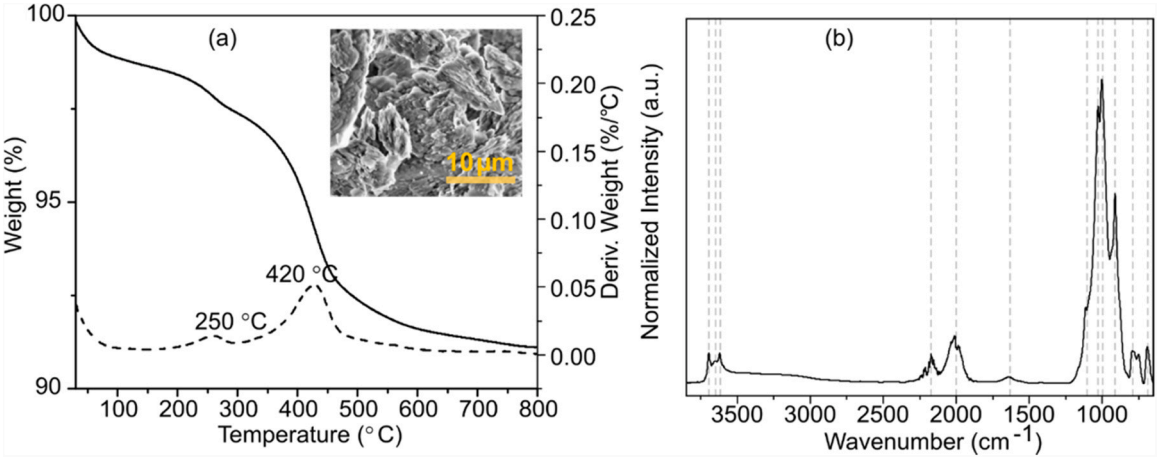


**Fig. 2.** (a) Thermogravimetric analysis curve (solid line) and DTG curve (dashed line) of lateritic soil at a heating rate of 5 °C/min under $N_2$ flow, and its structural morphology (inset), and (b) FTIR spectrum.

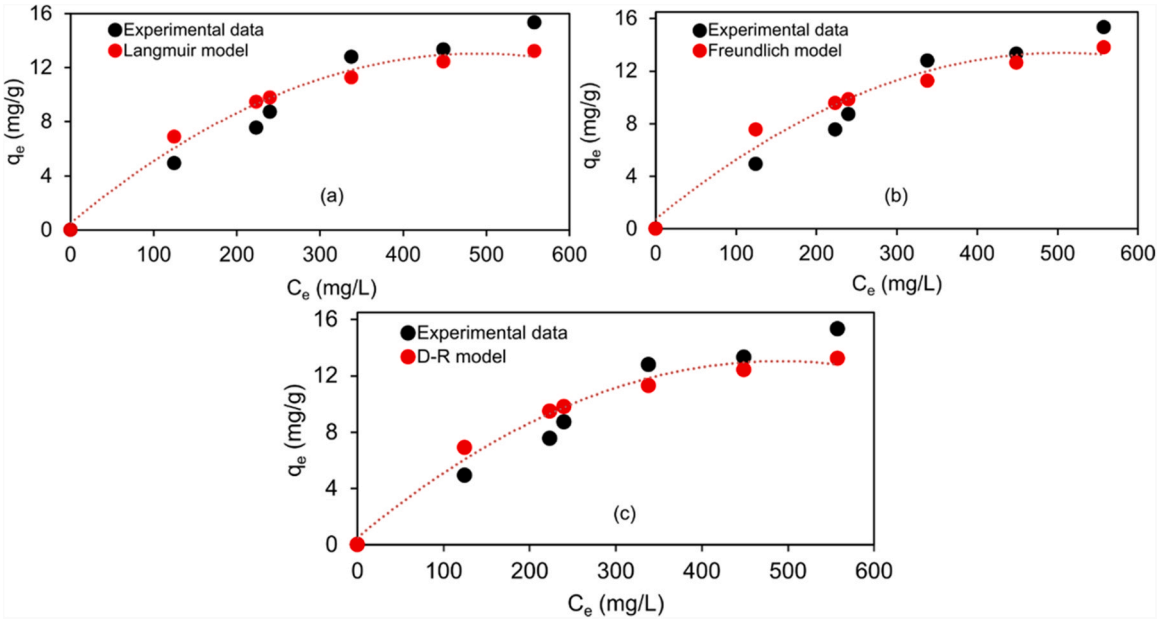


**Fig. 3.** (a) Langmuir, (b) Freundlich, and (c) D-R isotherm model fits of lateritic soil.

internal adsorption sites. However, the diffusion of the solute ions into the bulk of the adsorbent reduces towards equilibrium. In a study by Bhattacharjee et al. (2021) using LS as an adsorbent for the removal of P from sewage effluent, an initial rapid solute uptake was observed, followed by a gradual decline and finally a steady state condition where negligible uptake of the solutes occurred. These authors attributed the initial rapid mass transfer of the phosphates to the adsorption sites to a high ionic gradient. Moreover, the slow rate of phosphate sorption after equilibrium could have also originated from an increase in the total negative charge on the LS surface causing the repulsion of the anionic phosphates in the solution. Özacar (2003) reported that the adsorption of P onto calcined alunite increased with time but remained constant after 120 min. The author attributed the single, smooth, and continuous time profile curve of the uptake of P to the possible monolayer adsorption on the surface of the adsorbent. This is in conformity with the results from the present study where Langmuir equation provided the best fit to the isotherm data indicating a monolayer adsorption.

### 3.4. Effect of the initial concentration of P in urine on the amount adsorbed by LS

Equilibrium studies were conducted to evaluate the adsorption capacity of P ($q_e$) on LS using different initial concentrations, 164.12, 283.55, 309.82, 439.95, 555.04, and 680.21 mg/L at room temperature (21 °C), see Fig. 5.

**Table 3**
Langmuir, Freundlich, and D-R isotherm parameters for the adsorption of P on LS.

| Isotherm parameters | |
|---|---|
| Langmuir | |
| $q_{max}$ (mg/g) | 15.5 |
| $K_L$ | 0.006 |
| $R_L$ | 0.5 |
| $R^2$ | 0.991 |
| Freundlich | |
| $K_f$ | 1.1 |
| 1/n | 0.4 |
| $R^2$ | 0.996 |
| Dubinin-Radushkevich (D-R) | |
| $q_s$ (mg/g) | 14.0 |
| $K_{DR}$ | 0.003 |
| E (kJ/mol) | $1.313 \times 10^{-2}$ |
| $R^2$ | 0.999 |

The increasing amount of the adsorbed P at equilibrium ($q_e$) with increase in the initial concentration could be due to more ions being progressively available to attach themselves on to the adsorption sites (Fig. 5). Also, the higher ionic gradient between the adsorption surface and the solution at higher concentrations could lead to higher mass transfer of phosphate ions to the adsorption surface and consequently higher uptake of P. Similar results have been reported by Ramakrishnaiah (2012) in a study of phosphate adsorption on low-cost adsorbents. The author remarked that higher mass flow of ions to the adsorption sites occurs at elevated solute concentrations than at low concentrations. Wei et al. (2008) also found that phosphorous adsorption capacity of acid mine drainage sludge ranged from 9.89 to 31.97 mg/g when the concentration of municipal wastewater effluent was increased from 0.21 to 13.61 mg/L. The authors argued that increasing the concentration of the anionic phosphate ions in the solution enhanced the electrostatic attraction between the ions and the positively charged surfaces of sludge particles.

### 3.5. Optimization of the adsorption of P on LS

#### 3.5.1. Response surface methodology (RSM) experiment

The response surface methodology (RSM) was carried out to optimise the adsorption of P on LS and to investigate interactive effect of contact time, agitation speed and adsorbent loading. The optimisation modeling was performed at 21 °C, pH of 7.83 and initial concentration of P of 470.03 mg/L. The relationship between the response of adsorbed P and the three influencing variables, contact time, agitation speed, and adsorbent loadings considered in this study was analysed based on the central composite circumscribed design (CCCD) with each variable studied at 5 levels. The variations in the amount of the adsorbed P in different runs for both the predicted and actual responses indicate that the removal of P is strongly influenced by the variables considered in this study. The result of each run is displayed in Table 5.

As shown in Table 5, a wide range of adsorbed amount of P on LS from a minimum of 0.55 mg/g to a maximum of 132.73 mg/g occurred for the predicted responses, indicating a strong correlation between the adsorption of P and the contact time, speed, and loading. The estimated second-order quadratic response model equation in coded form was determined and evaluated to explain the adsorption behavior of P using

**Table 4**
Adsorption of P on lateritic soil compared with other adsorbents.

| Adsorbent | Solution | $q_{max}$ (mg/g) | Ref. |
|---|---|---|---|
| Lateritic soil | Sewage effluent | 384.61 | (Bhattacharjee et al., 2021) |
| Lateritic soil | Aqueous solution | 31.25 | (Hue and Tung, 2018) |
| Lateritic soil | Human urine | 15.5 | This study |
| Calcined alunite | Aqueous solution | 41.97 | (Özacar, 2003) |
| Bentonites | Aqueous solution | 9.80 | (Zhu et al., 2009) |
| Wood aspen fibres | Aqueous solution | 4.30 | (Eberhardt et al., 2006) |
| Fe –Mn binary oxide | Aqueous solution | 36 | (Zhang et al., 2009) |

"Design-Expert® software, version 12, Stat-Ease, Inc., Minneapolis, MN, USA, www.statease.com" which is presented in Eq. (11)

$$Y = 10.39 + 0.6112x_1 - 14.20x_2 - 32.83x_3 + 1.69x_1x_2 + 0.7538x_1x_3 + 16.25x_2x_3 + 4.96x_1^2 + 4.58x_2^2 + 23.73x_3^2 \quad (11)$$

where, $Y$ (mg/g) is the amount of the adsorbed P, $x_1$, $x_2$, and $x_3$ are the coded terms for contact time, agitation speed, and adsorbent loading, respectively.

The predicted amount of the adsorbed P for each run presented in Table 5 was obtained by solving Eq. (11).

### 3.5.2. ANOVA analysis and reliability of the RSM model

The analysis of variance (ANOVA) was conducted to study the significance of the quadratic model, while the value of the coefficient of determination ($R^2$) was used to determine the reliability of the quadratic model in fitting the experimental data and accurately predicting the output. The quadratic model had $R^2$ value of 0.972 implying that approximately 97.2 % of the variance in the experimental data is attributed to the variables investigated. The quadratic model was therefore adequate in predicting the amount of adsorbed P under the given experimental conditions since only 2.84 % of the total variations could not be accounted for by the quadratic model. Moreover, the difference between the predicted $R^2$ (0.782) and adjusted $R^2_{adj}$ (0.947) was $< 0.2$ suggesting that the predicted values (response) matched well with the observed ones, implying that the regression model had an excellent stability (Myers et al., 2004). The ANOVA results for the response surface quadratic model for the adsorption of P are presented in Table 6.

The results show that the quadratic model is statistically significant at 95 % confidence level, with F-value of 39.05 and very low probability p-value of $< 0.0001$, i.e., there is less than 0.01 % chance that the output response is due to noise. The reliability and validity of the RSM model was further investigated by the diagnostic plots presented in Fig. S1 (a–c). From the plots, the Normal Plot of Residuals (Fig. S1a), and Predicted vs. Actual (Fig. S1c) were both straight lines; while, the Residuals vs. Predicted (Fig. S1b), and Residuals vs. Run (Fig. S1d) were scattered randomly. From the results, it can therefore be seen that the model is suitable for use and can be used to identify the optimal conditions for achieving the highest removal of P from human by LS. Based on the set criteria for the model to maximize the contact time, and minimize the agitation speed and adsorbent loading with the overall goal of maximizing the adsorbed P, the selected solution was a contact time of 60 min, agitation speed of 80 rpm, and adsorbent loading of 0.1 g which yielded a predicted maximum P adsorption of 105.12 mg/g with a desirability of 0.919.

The 3D graphical plots showing the interactive effects of contact time, agitation speed, and adsorbent loading on the adsorption of P are presented in the Figs. S2–S4 in the Supplementary information. Among the three factors, contact time, agitation speed, and adsorbent loading optimised for achieving optimal adsorption of P on LS, increasing the contact time did not depict any significant change in slope of the response surface curvature (Figs. S3 and S4). This corroborates the ANOVA results which showed no significant ($P > 0.05$) effect on uptake of P with increase in contact time. This implies that once the equilibrium is reached, no further adsorption can occur since all the active sites are occupied.

On the other hand, increasing the agitation speed beyond 80 rpm showed a gradual decline in the amount of the adsorbed P as depicted in the 3D graphs presented in Figs. S2 and S4 in the Supplementary information. We can draw parallels with a study by Geethakarthi and Phanikumar (2011) where the adsorption of reactive dyes on activated

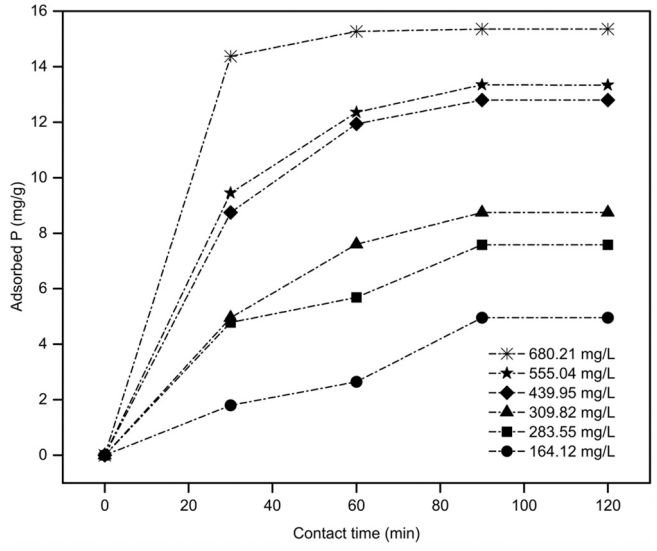


**Fig. 4.** The influence of contact time for adsorption of P on LS. The errors are smaller than the data marker. The lines drawn between the data points are a guide to the eye.

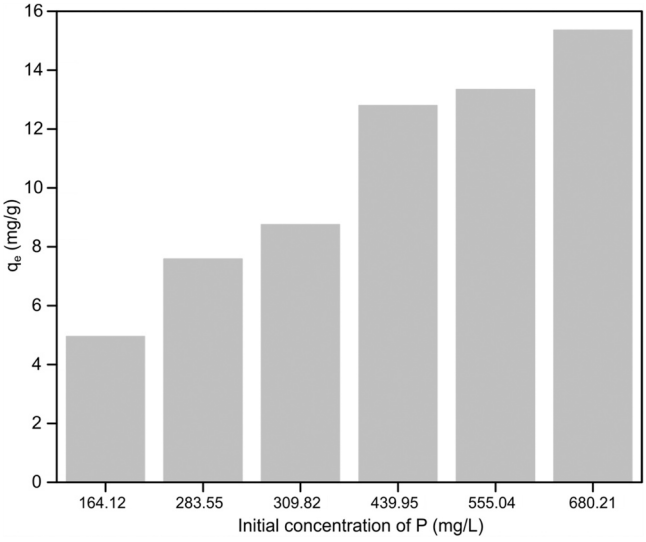


**Fig. 5.** Influence of the initial concentration of P in urine on the amount adsorbed by LS. The errors are below 1% for each data point.

**Table 5**
The central composite circumscribed design (CCCD) experiment and results.

| Coded values | | | | Actual values | | | Adsorbed phosphorous | |
|---|---|---|---|---|---|---|---|---|
| Run | $x_1$ | $x_2$ | $x_3$ | Contact time (min) | Speed (rpm) | Loading (g) | Actual (mg/g) | Predicted (mg/g) |
| **1** | 1.682 | 0 | 0 | 70 | 140 | 0.20 | 33.17 | 25.45 |
| **2** | 1 | -1 | -1 | 60 | 80 | 0.10 | 96.64 | 105.12 |
| **3** | -1 | 1 | -1 | 30 | 200 | 0.10 | 32.11 | 44.49 |
| **4** | 0 | 0 | 0 | 45 | 140 | 0.20 | 10.15 | 10.39 |
| **5** | 0 | -1.682 | 0 | 45 | 39 | 0.20 | 43.10 | 47.22 |
| **6** | 0 | 0 | 0 | 45 | 140 | 0.20 | 10.15 | 10.39 |
| **7** | 0 | 0 | 0 | 45 | 140 | 0.20 | 10.15 | 10.39 |
| **8** | 1 | 1 | 1 | 60 | 200 | 0.30 | 6.94 | 15.93 |
| **9** | -1.682 | 0 | 0 | 20 | 140 | 0.20 | 23.92 | 23.39 |
| **10** | -1 | -1 | 1 | 30 | 80 | 0.30 | 10.07 | 9.10 |
| **11** | 0 | 0 | -1.682 | 45 | 140 | 0.03 | 144.49 | 132.73 |
| **12** | 1 | -1 | 1 | 60 | 80 | 0.30 | 15.01 | 8.46 |
| **13** | 0 | 0 | 0 | 45 | 140 | 0.20 | 10.15 | 10.39 |
| **14** | 0 | 0 | 0 | 45 | 140 | 0.20 | 10.15 | 10.39 |
| **15** | 0 | 0 | 0 | 45 | 140 | 0.20 | 10.15 | 10.39 |
| **16** | 0 | 1.682 | 0 | 45 | 241 | 0.20 | 11.81 | 0.55 |
| **17** | -1 | 1 | 1 | 30 | 200 | 0.30 | 12.47 | 9.82 |
| **18** | 0 | 0 | 1.682 | 45 | 140 | 0.37 | 18.78 | 22.30 |
| **19** | -1 | -1 | -1 | 30 | 80 | 0.1 | 111.93 | 108.77 |
| **20** | 1 | 1 | -1 | 60 | 200 | 0.1 | 40.78 | 47.58 |

carbon was seen to decline with increase in the agitation speed beyond 120 rpm. The desorption or detachment of the adsorbed molecules at higher speed suggest that there is an optimal agitation speed or turbulence for any adsorption process. However, increasing the agitation speed gradually up to the optimum generally leads to a gradual increase in the amount of solutes adsorbed. For instance, Zahoor (2011) observed that the adsorption of imidacloprid on activated carbon increased with the agitation speed from 200 up to 300 rpm beyond which no significant increase in the adsorption occurred. The author argued that increasing turbulence decreases the boundary layer thickness surrounding the adsorbent particles leading to an increase in the accessibility of the available adsorption site. However, insignificant increase in the adsorption beyond 300 rpm implies that for any adsorption process, there is an optimum speed to achieve optimal adsorption, and thus should be investigated for every adsorbent.

The removal of solutes in aqueous phase will generally be affected by the adsorbent dosage since the adsorbents provide attachment sites. In our study, adsorbent dosage beyond 0.1 g led to a decline in the amount of the adsorbed P as shown by the 3D graphs in Figs. S2 and S3 in the Supplementary information. This is line with the work by Drenkova-Tuhtan et al. (2017), which reported a decrease in the removal of phosphates with increase in the adsorbent dose beyond the optimum dosage. The authors credited this observation to agglomeration of particles at higher dosage thereby reducing the accessibility of the active adsorption sites. In contrast, Xiong et al. (2011) reported that phosphate removal from aqueous solution increased with the amount of powdered freshwater mussel shells, an observation they attributed to an increase in the available surface area for attachment of phosphates. Based on the above discussion, it is worth pointing out that to achieve an optimal removal of solutes in any given fixed volume of a solution, the adsorption experiments should be carried out at optimum contact time, agitation speed and adsorbent dosage.

**Table 6**
ANOVA for response surface quadratic model.

| Source | F-value | p-value | |
|---|---|---|---|
| Model | 39.05 | < 0.0001 | Significant |
| $x_1$-contact time | 0.0643 | 0.8050 | Not significant |
| $x_2$-agitation speed | 34.71 | 0.0002 | Significant |
| $x_3$-adsorbent loading | 185.47 | < 0.0001 | Significant |
| $x_1x_2$ | 0.2866 | 0.6041 | Not significant |
| $x_1x_3$ | 0.0573 | 0.8157 | Not significant |
| $x_2x_3$ | 26.62 | 0.0004 | Significant |
| $x_1^2$ | 4.47 | 0.0606 | Not significant |
| $x_2^2$ | 3.80 | 0.0797 | Not significant |
| $x_3^2$ | 102.27 | < 0.0001 | Significant |

$R^2$, $R^2_{adj}$ (coefficient of determination) of the model is 0.972, 0.956, respectively.

## 4. Conclusions

To sum up, it can be inferred that the amount of the adsorbed P on LS at equilibrium ($q_e$) and pH = 7.5 increased with the initial concentration of P in urine as well as with the contact time. The presence of aluminium and iron in LS are associated with $Al_2O_3$ and $Fe_2O_3$ as seen by XRF, and the hydroxyl groups, Fe/Al-OH as detected by the FTIR analysis. It is therefore reasonable that a high surface-active site will be formed when the surface hydroxyl groups become positively charged through protonation, thus adsorbing electronegatively charged P through electrostatic forces with mean adsorption energy of $1.313 \times 10^{-2}$ kJ/mol as per the D-R model. This mechanism may well facilitate the high adsorption capacity of P of 15.5 mg/g obtained herein, a value that falls within the range of those previously reported in the literature. Also, the most desirable optimal conditions to attain the highest adsorption of P on LS (105.12 mg/g) were described by the RSM model as contact time of 60 min, agitation speed of 80 rpm, and adsorbent loading of 0.1 g. This process shows a potential of increasing the practical efficacy of the adsorbent for P removal.

## Data Availability

Data will be made available on request.

## Declaration of Competing Interest

The authors declare that they have no known competing financial interests or personal relationships that could have appeared to influence the work reported in this paper.

## Acknowledgement

This work was supported by the Erasmus+ Programme (Grant no. KA107-2017). We are grateful to the Department of Biological and

Environmental Science at the University of Jyvaskyla, Finland for the facilities used in conducting the adsorption experiments. Material characterization was performed at the Department of Chemistry – Ångström Laboratory, Uppsala University, Sweden.

## Appendix A. Supporting information

Supplementary data associated with this article can be found in the online version at doi:10.1016/j.clwas.2023.100081.

## References


Abdullah, M.A., Chiang, L., Nadeem, M., 2009. Comparative evaluation of adsorption kinetics and isotherms of a natural product removal by Amberlite polymeric adsorbents. Chem. Eng. J. 146, 370–376. https://doi.org/10.1016/j.cej.2008.06.018

Ayawei, N., Ebelegi, A.N., Wankasi, D., 2017. Modelling and interpretation of adsorption isotherms. J. Chem. 2017. https://doi.org/10.1155/2017/3039817

Beusen, A.H.W., Bouwman, A.F., Van Beek, L.P.H., Mogollón, J.M., Middelburg, J.J., 2016. Global riverine N and P transport to ocean increased during the 20th century despite increased retention along the aquatic continuum. Biogeosciences 13, 2441–2451. https://doi.org/10.5194/bg-13-2441-2016

Bhattacharjee, A., Jana, B.B., Mandal, S.K., Lahiri, S., Bhakta, J.N., 2021. Assessing phosphorus removal potential of laterite soil for water treatment and eco-technological application. Ecol. Eng. 166, 106245. https://doi.org/10.1016/j.ecoleng.2021.106245

Biswas, B.K., Inoue, K., Ghimire, K.N., Harada, H., Ohto, K., Kawakita, H., 2008. Removal and recovery of phosphorus from water by means of adsorption onto orange waste gel loaded with zirconium. Bioresour. Technol. 99, 8685–8690. https://doi.org/10.1016/j.biortech.2008.04.015

Boujelben, N., Bouzid, J., Elouear, Z., Feki, M., Jamoussi, F., Montiel, A., 2008. Phosphorus removal from aqueous solution using iron coated natural and engineered sorbents. J. Hazard. Mater. 151, 103–110. https://doi.org/10.1016/j.jhazmat.2007.05.057

Chittoo, B.S., Sutherland, C., 2014. Adsorption of phosphorus using water treatment sludge. J. Appl. Sci. 14, 3455–3463. https://doi.org/10.3923/jas.2014.3455.3463

Drenkova-Tuhtan, A., Schneider, M., Franzreb, M., Meyer, C., Gellermann, C., Sextl, G., Mandel, K., Steinmetz, H., 2017. Pilot-scale removal and recovery of dissolved phosphate from secondary wastewater effluents with reusable ZnFeZr adsorbent @ Fe3O4/SiO2 particles with magnetic harvesting. Water Res. 109, 77–87. https://doi.org/10.1016/j.watres.2016.11.039

Eberhardt, T.L., Min, S.H., Han, J.S., 2006. Phosphate removal by refined aspen wood fiber treated with carboxymethyl cellulose and ferrous chloride. Bioresour. Technol. 97, 2371–2376. https://doi.org/10.1016/j.biortech.2005.10.040

Edokpayi, J.N., Odiyo, J.O., Durowoju, O.S., 2017. Impact of wastewater on surface water quality in developing countries: a case study of South Africa. Water Qual. https://doi.org/10.5772/66561

Finnish Standards SFS 3026, 1986. Finnish Standard for Determination of Total Phosphorus in Water. Digestion with Peroxodisulfate. Finnish Standards Association, Helsinki, Finland.

Foo, K.Y., Hameed, B.H., 2010. Insights into the modeling of adsorption isotherm systems. Chem. Eng. J. 156, 2–10. https://doi.org/10.1016/j.cej.2009.09.013

Fulazzaky, M.A., Khamidun, M.H., Din, M.F.M., Yusoff, A.R.M., 2014. Adsorption of phosphate from domestic wastewater treatment plant effluent onto the laterites in a hydrodynamic column. Chem. Eng. J. 258, 10–17. https://doi.org/10.1016/j.cej.2014.07.092

Geethakarthi, A., Phanikumar, B.R., 2011. Adsorption of reactive dyes from aqueous solutions by tannery sludge developed activated carbon: kinetic and equilibrium studies. Int. J. Environ. Sci. Technol. 8, 561–570.

Glocheux, Y., Pasarín, M.M., Albadarin, A.B., Allen, S.J., Walker, G.M., 2013. Removal of arsenic from groundwater by adsorption onto an acidified laterite by-product. Chem. Eng. J. 228, 565–574. https://doi.org/10.1016/j.cej.2013.05.043

Hameed, B.H., El-Khaiary, M.I., 2008. Malachite green adsorption by rattan sawdust: isotherm, kinetic and mechanism modeling. J. Hazard. Mater. 159, 574–579. https://doi.org/10.1016/j.jhazmat.2008.02.054

Hu, Q., Zhang, Z., 2019. Application of Dubinin–Radushkevich isotherm model at the solid/solution interface: a theoretical analysis. J. Mol. Liq. 277, 646–648. https://doi.org/10.1016/j.molliq.2019.01.005

Hue, N.T., Tung, N.H., 2018. Study on simultaneous adsorption of phosphate and fluoride from water environment by modified laterite ore from Northern Vietnam. Green Process. Synth. 7, 89–99. https://doi.org/10.1515/gps-2016-0136

Jeon, D.J., Yeom, S.H., 2009. Recycling wasted biomaterial, crab shells, as an adsorbent for the removal of high concentration of phosphate. Bioresour. Technol. 100, 2646–2649. https://doi.org/10.1016/j.biortech.2008.11.035

Jeppesen, T., Shu, L., Keir, G., Jegatheesan, V., 2009. Metal recovery from reverse osmosis concentrate. J. Clean. Prod. 17, 703–707. https://doi.org/10.1016/j.jclepro.2008.11.013

Kakali, G., Perraki, T., Tsivilis, S., Badogiannis, E., 2001. Thermal treatment of kaolin: the effect of mineralogy on the pozzolanic activity. Appl. Clay Sci. 20, 73–80. https://doi.org/10.1016/S0169-1317(01)00040-0

Kamtchueng, B.T., Onana, V.L., Fantong, W.Y., Ueda, A., Ntouala, R.F., Wongolo, M.H., Ndongo, G.B., Ze, A.N., Kamgang, V.K., Ondoa, J.M., 2015. Geotechnical, chemical and mineralogical evaluation of lateritic soils in humid tropical area (Mfou, Central-Cameroon): implications for road construction. Int. J. Geo-Eng. 6, 1–21. https://doi.org/10.1186/s40703-014-0001-0

Karak, T., Bhattacharyya, P., 2011. Human urine as a source of alternative natural fertilizer in agriculture: a flight of fancy or an achievable reality. Resour. Conserv. Recycl. 55, 400–408. https://doi.org/10.1016/j.resconrec.2010.12.008

Kisinyo, P.O., Opala, P.A., Gudu, S.O., Othieno, C.O., Okalebo, J.R., Palapala, V., Otinga, A.N., 2014. Recent advances towards understanding and managing Kenyan acid soils for improved crop production. Afr. J. Agric. Res. 9, 2397–2408. https://doi.org/10.5897/ajar2013.8359

Ko, T.H., 2014. Nature and properties of lateritic soils derived from different parent materials in Taiwan. Sci. World J. 2014. https://doi.org/10.1155/2014/247194

Larsen, T.A., Gujer, W., 1996. Separate management of anthropogenic nutrient solutions (human urine). Water Sci. Technol. 34, 87–94. https://doi.org/10.1016/0273-1223(96)00560-4

Lemougna, P.N., Madi, A.B., Kamseu, E., Melo, U.C., Delplancke, M.P., Rahier, H., 2014. Influence of the processing temperature on the compressive strength of Na activated lateritic soil for building applications. Constr. Build. Mater. 65, 60–66. https://doi.org/10.1016/j.conbuildmat.2014.04.100

Li, J., Ma, C., Ma, Y., Li, Y., Zhou, W., Xu, P., 2007. Medium optimization by combination of response surface methodology and desirability function: an application in glutamine production. Appl. Microbiol. Biotechnol. 74, 563–571. https://doi.org/10.1007/s00253-006-0699-5

López, E., Soto, B., Arias, M., Núñez, A., Rubinos, D., Barral, M.T., 1998. Adsorbent properties of red mud and its use for wastewater treatment. Water Res. 32, 1314–1322. https://doi.org/10.1016/S0043-1354(97)00326-6

Mahmoud, M.A., 2015. Kinetics and thermodynamics of aluminum oxide nanopowder as adsorbent for Fe (III) from aqueous solution. Beni-Suef Univ. J. Basic Appl. Sci. 4, 142–149. https://doi.org/10.1016/j.bjbas.2015.05.008

Martin, T.M.P., Esculier, F., Levavasseur, F., Houot, S., 2020. Human urine-based fertilizers: a review. Crit. Rev. Environ. Sci. Technol. 0, 1–47. https://doi.org/10.1080/10643389.2020.1838214

Maurer, M., Pronk, W., Larsen, T.A., 2006. Treatment processes for source-separated urine. Water Res. 40, 3151–3166. https://doi.org/10.1016/j.watres.2006.07.012

Mitra, S., Thakur, L.S., Rathore, V.K., Mondal, P., 2016. Removal of Pb(II) and Cr(VI) by laterite soil from synthetic waste water: single and bi-component adsorption approach. Desalin. Water Treat. 57, 18406–18416. https://doi.org/10.1080/19443994.2015.1088806

Mohamed, A.M.O., 2002. Development of a novel electro-dialysis based technique for lead removal from silty clay polluted soil. J. Hazard. Mater. 90, 297–310. https://doi.org/10.1016/S0304-3894(01)00361-2

Myers, R.H., Montgomery, D.C., Geoffrey Vining, G., Borror, C.M., Kowalski, S.M., 2004. Response surface methodology: a retrospective and literature survey. J. Qual. Technol. 36, 53–78. https://doi.org/10.1080/00224065.2004.11980252

Oguz, E., 2005. Sorption of phosphate from solid/liquid interface by fly ash. Colloids Surf. A Physicochem. Eng. Asp. 262, 113–117. https://doi.org/10.1016/j.colsurfa.2005.04.016

Osei, J., Gawu, S.K., Schäfer, A.I., Atipoka, F.A., Momade, F.W., 2016. Impact of laterite characteristics on fluoride removal from water. J. Chem. Technol. Biotechnol. 91, 911–920. https://doi.org/10.1002/jctb.4656

Otieno, A.O., Home, P.G., Raude, J.M., Murunga, S.I., Ngumba, E., Ojwang, D.O., Tuhkanen, T., 2021. Pineapple peel biochar and lateritic soil as adsorbents for recovery of ammonium nitrogen from human urine. J. Environ. Manag. 293, 112794. https://doi.org/10.1016/j.jenvman.2021.112794

Özacar, M., 2003. Equilibrium and kinetic modelling of adsorption of phosphorus on calcined alunite. Adsorption 9, 125–132. https://doi.org/10.1023/A:1024289209583

Preisner, M., Neverova-Dziopak, E., Kowalewski, Z., 2021. Mitigation of eutrophication caused by wastewater discharge: a simulation-based approach. Ambio 50, 413–424. https://doi.org/10.1007/s13280-020-01346-4

Ragheb, S.M., 2013. Phosphate removal from aqueous solution using slag and fly ash. HBRC J. 9, 270–275. https://doi.org/10.1016/j.hbrcj.2013.08.005

Ramakrishnaiah, V., 2012. Removal of phosphate from wastewater using low-cost adsorbents. Int. J. Eng. Invent. 1, 44–50.

Razali, M., Zhao, Y.Q., Bruen, M., 2007. Effectiveness of a drinking-water treatment sludge in removing different phosphorus species from aqueous solution. Sep. Purif. Technol. 55, 300–306. https://doi.org/10.1016/j.seppur.2006.12.004

Rocha, J., Klinowski, J., 1990. 29Si and 27Al magic-angle-spinning NMR studies of the thermal transformation of kaolinite. Phys. Chem. Miner. 17, 179–186. https://doi.org/10.1007/BF00199671

Sarkar, M., Banerjee, A., Pramanick, P.P., Sarkar, A.R., 2006. Use of laterite for the removal of fluoride from contaminated drinking water. J. Colloid Interface Sci. 302, 432–441. https://doi.org/10.1016/j.jcis.2006.07.001

Stoops, G., Marcelino, V., 2018. Lateritic and bauxitic materials. In: Interpretation of Micromorphological Features of Soils and Regoliths. Elsevier, pp. 691–720. https://doi.org/10.1016/b978-0-444-63522-8.00024-3

Tanada, S., Kabayama, M., Kawasaki, N., Sakiyama, T., Nakamura, T., Araki, M., Tamura, T., 2003. Removal of phosphate by aluminum oxide hydroxide. J. Colloid Interface Sci. 257, 135–140. https://doi.org/10.1016/S0021-9797(02)00008-5

Udert, K.M., Larsen, T.A., Gujer, W., 2006. Fate of major compounds in source-separated urine. Water Sci. Technol. 54, 413–420. https://doi.org/10.2166/wst.2006.921

Van Vuuren, D.P., Bouwman, A.F., Beusen, A.H.W., 2010. Phosphorus demand for the 1970–2100 period: a scenario analysis of resource depletion. Glob. Environ. Change 20, 428–439. https://doi.org/10.1016/j.gloenvcha.2010.04.004

Wei, X., Viadero, R.C., Bhojappa, S., 2008. Phosphorus removal by acid mine drainage sludge from secondary effluents of municipal wastewater treatment plants. Water Res. 42, 3275–3284. https://doi.org/10.1016/j.watres.2008.04.005

Wilsenach, J.A., Schuurbiers, C.A.H., van Loosdrecht, M.C.M., 2007. Phosphate and potassium recovery from source separated urine through struvite precipitation. Water Res. 41, 458–466. https://doi.org/10.1016/j.watres.2006.10.014

Wu, D., Zhang, B., Li, C., Zhang, Z., Kong, H., 2006. Simultaneous removal of ammonium and phosphate by zeolite synthesized from fly ash as influenced by salt treatment. J. Colloid Interface Sci. 304, 300–306. https://doi.org/10.1016/j.jcis.2006.09.011

Xiong, J., Qin, Y., Islam, E., Yue, M., Wang, W., 2011. Phosphate removal from solution using powdered freshwater mussel shells. Desalination 276, 317–321. https://doi.org/10.1016/j.desal.2011.03.066

Xu, X., Gao, B., Yue, Q., Zhong, Q., 2011. Sorption of phosphate onto giant reed based adsorbent: FTIR, Raman spectrum analysis and dynamic sorption/desorption properties in filter bed. Bioresour. Technol. 102, 5278–5282. https://doi.org/10.1016/j.biortech.2010.10.130

Yadav, M.K., Gupta, A.K., Ghosal, P.S., Mukherjee, A., 2017. pH mediated facile preparation of hydrotalcite based adsorbent for enhanced arsenite and arsenate removal: insights on physicochemical properties and adsorption mechanism. J. Mol. Liq. 240, 240–252. https://doi.org/10.1016/j.molliq.2017.05.082

Yamada, H., Kayama, M., Saito, K., Hara, M., 1986. A fundamental research on phosphate removal by using slag. Water Res. 20, 547–557. https://doi.org/10.1016/0043-1354(86)90018-7

Yaneva, Z.L., Koumanova, B.K., Georgieva, N.V., 2013. Linear and nonlinear regression methods for equilibrium modelling of p-nitrophenol biosorption by Rhizopus oryzae: comparison of error analysis criteria. J. Chem. 2013. https://doi.org/10.1155/2013/517631

Yang, Y., Tomlinson, D., Kennedy, S., Zhao, Y.Q., 2006. Dewatered alum sludge: a potential adsorbent for phosphorus removal. Water Sci. Technol. 54, 207–213. https://doi.org/10.2166/wst.2006.564

Yuh-Shan, H., 2006. Isotherms for the sorption of lead onto peat: comparison of linear and non-linear methods. Pol. J. Environ. Stud. 15, 81–86.

Zahoor, M., 2011. Effect of agitation speed on adsorption of imidacloprid on activated carbon. J. Chem. Soc. Pak. 33, 305.

Zhang, G., Liu, H., Liu, R., Qu, J., 2009. Removal of phosphate from water by a Fe-Mn binary oxide adsorbent. J. Colloid Interface Sci. 335, 168–174. https://doi.org/10.1016/j.jcis.2009.03.019

Zhang, L., Hong, S., He, J., Gan, F., Ho, Y.S., 2011. Adsorption characteristic studies of phosphorus onto laterite. Desalin. Water Treat. 25, 98–105. https://doi.org/10.5004/dwt.2011.1871

Zhu, R., Zhu, L., Zhu, J., Ge, F., Wang, T., 2009. Sorption of naphthalene and phosphate to the CTMAB-Al13 intercalated bentonites. J. Hazard. Mater. 168, 1590–1594. https://doi.org/10.1016/j.jhazmat.2009.03.057